Article

Igneous Records of Mongolia–Okhotsk Ocean Subduction: Evidence from Granitoids in the Greater Khingan Mountains

Jixu Liu, Cui Liu *, Jinfu Deng, Zhaohua Luo, Guoqi He and Qing Liu

School of Earth Sciences and Resources, China University of Geosciences, Beijing 100083, China
* Correspondence: liucui@cugb.edu.cn

Abstract: Large-scale Mesozoic granitoids are exposed in the Greater Khingan Mountains. Their relationship with the Mongolia–Okhotsk and the Paleo-Pacific Ocean is still under discussion and a matter of debate. In this study, field observations were made and a total of 18 granitoids exposed in the vicinity of the Heihe–Baishilazi area in the northern part of the Greater Khingan Mountains were sampled for petrological, geochronological, and geochemical research. In addition, to complement this study, 90 granitic samples from the Xinghua, Dajinshan, Yili, Chabaqi, and Sankuanggou areas in the Greater Khingan Mountains were compiled in order to reveal rock assemblages, magma sources, and then inquire into the tectonic background. Zircon LA–ICP–MS U–Pb dating indicates that two samples from the Heihe area were formed in the Early Jurassic period (194.2 ± 1.4 Ma and 183.1 ± 1.3 Ma), and the εHf(t) values and TDM_2 of the zircons were mainly +5.8 to +10.7 and 528 Ma to 834 Ma, respectively, with a large variation range. The intrusive rocks from the Greater Khingan Mountains (108 in total) belonging to the $T_1T_2G_1G_2$ assemblage contained tonalites (T_1), trondhjemites (T_2), granodiorites (G_1), and granites (G_2). These granitoids are presented as subalkaline series in a plot of total alkali versus SiO_2 (TAS diagram), medium-K calc-alkaline and high-K calc-alkaline series on SiO_2 versus K_2O diagram, with metaluminous to peraluminous characteristics on an A/CNK versus A/NK diagram. These are shown as a MA (magnesium andesite) series and LMA (lower (or non) magnesium andesite) series on a SiO_2 versus MgO diagram, which can be further divided into the higher-pressure TTG subtype of the MA (corresponding to high-SiO_2 adakite (HSA)) series and the lower-pressure TTG subtype of LMA (corresponding to typical calc-alkaline suprasubduction zone rocks). In addition, granitoids were enriched in light rare earth elements (LREEs) and large ion lithophile elements (LILEs) and depleted in heavy rare earth elements (HREEs) and high-field-strength elements (HFSEs), corroborating a suprasubduction zone environment. Regional correlations as well as geochemical characteristics indicate that the rocks from the Greater Khingan Mountains formed in a subduction zone environment during the Early Jurassic; primary magma had presumably originated from the melting of young and hot oceanic crust under eclogite to amphibolite facies conditions. According to the spatial variation in rock assemblages ($T_1T_2G_1$ to G_1G_2 and G_2), we speculate that the northeastern Heihe, Baishilazi, and Xinghua areas as well as the westward Dajinshan area were adjacent to the ocean and formed an outer subduction zone, whereas the southwestward Sankuanggou, Yili, and Chabaqi areas were adjacent to the continent, forming an inner subduction zone. The distribution sites of the inner and outer subduction zones indicate southward and southwestward ocean subduction. Therefore, we propose a direct connection with southward subduction of the Mongolia–Okhotsk Ocean.

Keywords: Early Jurassic; rock assemblages; magma source; Mongolia–Okhotsk Ocean subduction; the Greater Khingan Mountains

1. Introduction

The Mongolia–Okhotsk suture zone is mainly distributed between 96° and 130° E longitudes and 46° and 58° N latitudes in Russia and Mongolia. It ranges from the Khangay Mountains of Central Mongolia in the west to Uda Gulf of the Okhotsk Sea in the east [1], roughly along the Ulaanbaatar, Baikal, and Okhotsk Sea, with a NE–SW strike [2]. There have been a few previous studies on the influence of the Mongolia–Okhotsk Ocean in NE China, while some hypothesize that the Mesozoic magmatism–tectonism–mineralization systems in NE China have a relationship with the Paleo-Pacific Ocean. Wu et al. [3] suggested that the formation of Jurassic granitoids in NE China was related to the subduction of the Paleo-Pacific plate. Xu et al. [4] indicated that the Early Cretaceous volcanic rocks in Heilongjiang and Jilin Province were subjected to low-angle subduction of the Paleo-Pacific plate under the Eurasian continent. In addition, the deposits formed from 210 Ma to 170 Ma such as Luming, Daheishan, Wudaoling, and Sankuanggou were related to the Paleo-Pacific tectonic system [5,6]. Mesozoic magmatic activities in NE China are widespread [3,7] and have created large-scale intrusive magmatic bodies. Wu et al. [3] proposed that NE China was characterized by a large amount of granitoids with a distribution area exceeding 200,000 km^2. There are different ideas about the ages of the formation and assemblages of these huge large intrusive bodies; as a result, there is still considerable debate about the petrogenesis of these rocks [3,8–11]. For instance, magma was presumably derived from thickened lithosphere delamination, leading to asthenosphere upwelling and underplating [3,7,12], partial melting of the subducting oceanic crust and basaltic lower crust [6,13,14], partial melting of a depleted mantle wedge that had been metasomatized by fluids derived from a subducted slab [15], and so on. The influences of the Mongolia–Okhotsk or the Paleo-Pacific Ocean [3,4,14,16–19] on the Greater Khingan Mountains during the Mesozoic are still worth researching. In order to reveal the petrogenesis of large-scale granitoids in the Greater Khingan Mountains, and to determine the direction of ocean subduction, it is necessary to clarify the spatial distribution characteristics of rock assemblages, magma sources, and tectonic backgrounds in this region. Therefore, this study focused on the granitoids in the Greater Khingan Mountains region with the aim to enrich the basic geological research, providing reliable data for further research on granites and related mineral explorations.

2. Geological Background

The study area is located in the Greater Khingan Mountains, which also belongs to the Xing'an massif. The Xing'an massif is an important tectonic unit in the eastern section of the Central Asian Orogenic Belt (CAOB) (Figure 1). It amalgamated with the Erguna massif in the Early Paleozoic Era (approximately 500 Ma) [20,21], and might have been amalgamated with the Songnen–Zhangguangcai Range before the Permian [16] or before the end of the Early Carboniferous periods [22]. The Xing'an massif is bounded by the Xiguitu–Tayuan fault to the northwest and the Hegenshan–Heihe fault to the southeast [8] (Figure 2).

The major exposures in the northern Greater Khingan Mountains are shown in Table 1. Carboniferous and Permian granitoids are only sporadically distributed, while Mesozoic granitoids are widely exposed around the northeastern Xing'an massif [3].

Large tectonic lines were mainly in the EW direction before the Late Triassic period, changing to the NE direction during the Early Jurassic [25]. Large-scale faults included the Tayuan–Xiguitu fault and Hegenshan–Heihe fault [8,24].
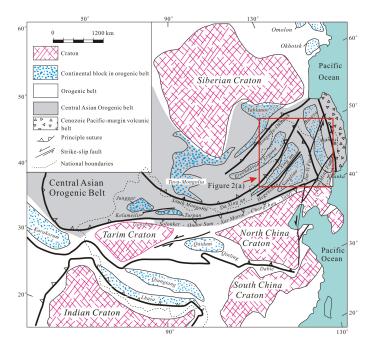
Figure 1. Simplified tectonic diagram showing the main units of central and eastern Asia (modified after [20]).
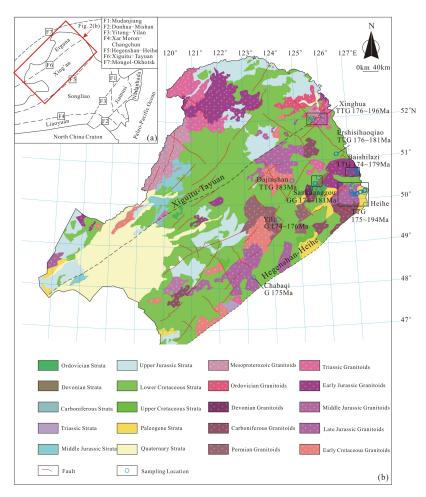

Figure 2. (**a**) Simplified tectonic sketch map of NE China [3]. (**b**) Geological sketch map of NE China (modified after [23]). TTG—tonalite–trondhjemite–granodiorite; GG—granodiorite–granite; G—granite.

Table 1. Major exposure stratum in the northern Greater Khingan Mountains [10,11,24].

Eonothem	Erathem	System	Group/Formation	Symbol
Phanerozoic	Cenozoic	Paleogene–Neogene	Sunwu Formation	E_3N_2s
	Mesozoic	Cretaceous	Jiufengshan Formation	K_1j
			Guanghua Formation	K_1gn
			Longjiang Formation	K_1l
		Jurassic	Qilinhe Formation	J_2q
		Triassic	Laolongtou Formation	T_1l
	Paleozoic	Permian	Huaduoshan Formation	P_3h
		Carboniferous	Huadaqi Formation	C_1h
		Silurian–Devonian	Niqiuhe Formation	S_3D_2n
		Silurian	Woduhe Formation	S_3w
			Huanghuagou Formation	S_1h
		Ordovician	Luohe Formation	O_3l
			Duobaoshan Formation	O_2d
			Tongshan Formation	$O_{1-2}t$
Proterozoic	Neoproterozoic		Luomahu Group	Pt_3b/Pt_3g
	Paleoproterozoic		Xinghuadukou Group	Pt_1Xh

3. Sample Descriptions

Field geological observations and samplings were carried out around the Heihe and Baishilazi areas, and 18 samples in total were collected in the field. We also compiled the geochronological and geochemical data of 90 granitoids from previous studies around the Greater Khingan Mountains region [6,8,10,24,26–34] (see Figure 2 for the sampling locations).

Sample HEIH2018726–6, quartz monzonite, was collected from a stock that was not mapped in the 1:250,000 geological map of Heihe City, Research Institute of Regional Geological Survey of Heilongjiang [11]; the sampling site is located close to the Heihe to Luoguhe (Heiluo) National Road (50°14′48.32″ N, 127°23′31.99″ E, altitude: 216 m). The quartz monzonite is gray, exhibits a middle-fine-grained texture and a massive structure (Figure 3a), and consists of orthoclase (~35%, 2~3 mm), plagioclase (~35%, 1~1.5 mm), quartz (~12%, 0.5 mm), biotite (~10%, 0.5 mm), some opaque metal minerals, and accessory minerals including zircon and titanite. Some orthoclase grains have Carlsbad twins, and plagioclase grains show polysynthetic twins; quartz grains are anhedral (Figure 4a).
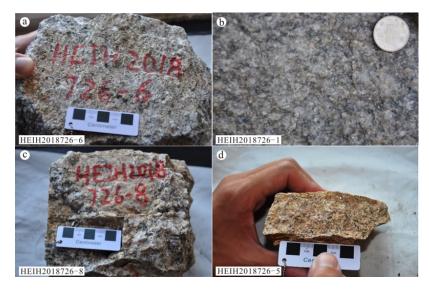

Figure 3. Field photographs of the granitoids: (**a**) quartz monzonite, (**b**) quartz monzonite, (**c**) porphyritic granite, (**d**) syenogranite.
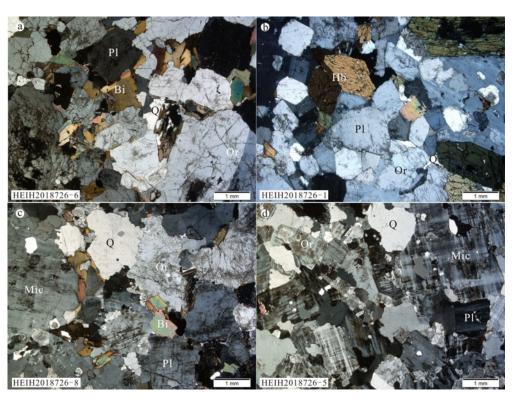
Figure 4. Photomicrographs of granitoids: (**a**) quartz monzonite, (**b**) quartz monzonite, (**c**) porphyritic granite, and (**d**) syenogranite. Q, quartz; Or, orthoclase; Pl, plagioclase; Bi, biotite; Hb, hornblende; Mic, microcline (cross-polarized light).

Sample HEIH2018726–1, quartz monzonite, was collected from a stock mapped as T_3J_1 (Late Triassic to Early Jurassic) granodiorite during the 1:250,000 geological map of Heihe City [11]; the sampling site is adjacent to the G331 highway (50°15′50.07″ N, 127°25′21.26″ E, altitude: 158 m). The quartz monzonite is gray, exhibits middle-fine-grained granitic texture and a massive structure (Figure 3b), and comprises plagioclase (~30%, 1.5 mm), orthoclase (~30%, 1~1.5 mm), hornblende (~20%, 1.5~3 mm), quartz (10%, 0.2~0.5 mm), biotite (~5%, 0.3 mm), a small amount of opaque minerals, and accessory minerals. Plagioclase grains have polysynthetic twins; hornblende grains are generally euhedral and partially have twins and have undergone chloritization; quarte grains are anhedral and fill between other mineral particles (Figure 4b).

Sample HEIH2018726–8, porphyritic granite, was collected from the same site as sample HEIH2018726–6 (50°14′48.32″ N, 127°23′31.99″ E, altitude: 225 m). The porphyritic granite is gray, slightly weathered, and exhibits a porphyroid texture and a massive structure (Figure 3c). The phenocrysts are mainly quartz (~20%, 1~2 mm), plagioclase (~20%, 1~1.5 mm), microcline (~15%, 2~2.5 mm), and orthoclase (~15%, 1.5~2 mm). The groundmass comprises quartz (~10%), plagioclase (~8%), biotite (~5%), and minor accessory minerals (~3%) including zircon, titanite, and magnetite (Figure 4c).

Sample HEIH2018726–5, syenogranite, was collected from the Shitouren Reservoir near Heihe City (50°14′37.62″ N, 127°22′56.46″ E, altitude: 221 m). Syenogranite is gray–yellow in color, slightly weathered, and has a slightly oriented medium and fine-grained granitic texture as well as a massive structure (Figure 3d). It consists of microcline (~40%, 1~2.5 mm), quartz (~30%, 0.5~1.5 mm), plagioclase (~10%, 1 mm), orthoclase (~10%, 0.5~1 mm), biotite (~5%, 0.2 mm), and accessory minerals (~3%) including zircon and magnetite. Microcline grains show tartan twinning, and orthoclase grains have undergone kaolinization (Figure 4d).

4. Testing and Analysis

4.1. Analytical Procedure

4.1.1. Zircon U–Pb Dating

Zircons were separated from two samples (HEIH2018726–8 and HEIH2018726–6) by the Langfang Regional Geological Survey, Hebei Province, China, using standard techniques of density and magnetic separation, and then by handpicking under a binocular microscope to select the zircon grains. The handpicked zircon grains were examined under transmitted and reflected light with an optical microscope. Cathodoluminescence (CL) images were obtained using a JEOL JSM6510 scanning electron microscope fitted with a GATAN Chroma CL detector at Gaonianlinghang Company, Beijing City, China, to reveal their internal structures and choose potential targets for U–Pb dating. The samples were analyzed for U–Pb geochronology using an LA–ICP–MS apparatus housed at the Inner Mongolia Geological Survey, Hohhot, China. Zircon 91500 was used as an external standard for age calibration, and NIST SRM 610 silicate glass was applied for instrument optimization. Details on the instrument settings and analytical procedures have been published elsewhere [35]. Corrections for common Pb were performed following prior guidance [36]. The ICP–MS–DataCal (Ver. 6.7 [37]) programs were used for data reduction and Isoplot (Ver. 3.0; [38]) for the concordia diagrams.

4.1.2. Major and Trace Element Determinations

The samples for whole-rock major and trace element analyses were crushed in a jaw crusher; these were then ground to 200 mesh using an agate ball miller at the Langfang Regional Geological Survey, Hebei Province, China. Major elements and trace elements were analyzed at the State Key Laboratory of Isotope Geochemistry, Guangzhou Institute of Geochemistry, Chinese Academy of Sciences. Major elements were analyzed on a Rigaku ZXS100e X fluorescence spectrophotometer (XRF) and the analytical precision was better than 2%. Trace elements were determined by an Agilent7500a inductively coupled plasma–mass spectrometer (ICP–MS). Two standard samples (AGV–2, GSR–1) were used to ensure the accuracy, and the analytical precision was better than 5~10%.

4.1.3. Hf Isotope Analyses

In situ zircon Hf isotope analyses were performed using a Neptune multi-collector–inductively coupled plasma–mass spectrometer (MC–ICP–MS) with a Geolas HD 193 nm laser ablation system at the Analysis and Testing Center of the Inner Mongolia Geological Survey, Hohhot, China. Details of the analytical method and instrumental settings have been published elsewhere [39].

4.2. Analytical Result

4.2.1. Zircon U–Pb Dating

In this study, two samples (HEIH2018726–8 and HEIH2018726–6) were dated by the LA–ICP–MS zircon U–Pb method (see results in Table S1).

For the HEIH2018726-8 sample, porphyritic granite, nine zircons were selected for U–Pb dating. Zircons were euhedral–subhedral, and ranged in size from 100 mm to 200 mm in length with a length/width ratio of approximately 1.5:1 to 2.5:1. Most grains exhibited obvious oscillatory zoning in the cathodoluminescence images (Figure 5a), indicating an igneous origin [40]. We therefore considered the LA–ICP–MS zircon U–Pb age to represent the crystallization age of the rock. Zircon grains exhibited Th and U contents of 298–686 ppm and 364–989 ppm, respectively, with a Th/U value of 0.50–1.13; the ^{206}Pb/^{238}U ages from nine analytical spots of zircons ranged from 192 to 195 Ma, yielding a weighted mean ^{206}Pb/^{238}U age of 194.2 $\pm$ 1.4 Ma (MSWD = 0.71) (Figure 6a).
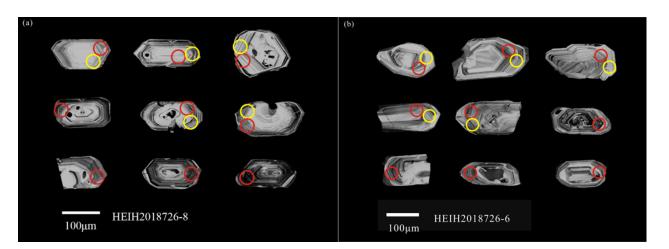
Figure 5. Cathodoluminescence (CL) images of the selected zircons for analysis from the Early Jurassic granitoids examined in the Greater Khingan Mountains (red circles indicate U–Pb dating points; yellow circles indicate Lu–Hf isotope points). (**a**) sample HEIH2018726-8, (**b**) sample HEIH2018726-6.
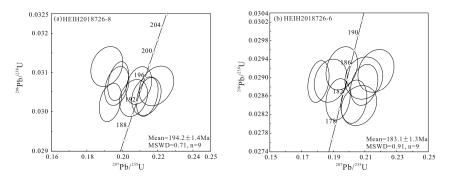

Figure 6. Zircon U–Pb concordia diagrams for the Early Jurassic granitoids examined in the Greater Khingan Mountains. (**a**) sample HEIH2018726-8, (**b**) sample HEIH2018726-6.

For sample HEIH2018726-6, a quartz monzonite, nine zircons were chosen for testing and analysis. Zircon grains are euhedral–subhedral, and range in size from 100 mm to 250 mm in length with a length/width ratio of approximately 1.5:1 to 3:1. The grains also exhibited oscillatory zoning in the CL image (Figure 5b). Their Th and U contents displayed ranges of 166–427 ppm and 235–479 ppm, respectively, with Th/U values of 0.62–1.13; the $^{206}Pb/^{238}U$ ages from nine analytical spots of zircons ranged from 179 to 186 Ma, yielding a weighted mean $^{206}Pb/^{238}U$ age of 183.1 ± 1.3 Ma (MSWD = 0.91) (Figure 6b), which could represent the crystallization age of the rock.

4.2.2. Major Elements

The major element data of granitoids are shown in Table S2. Samples were removed with a loss of ignition and volatiles, and geochemical diagrams were drawn after reconverting to 100%. The granitoids from Yili, Xinghua, and Dajinshan areas showed SiO_2 levels in the range of 61.46~74.52% (n = 31), TiO_2 levels in the range of 0.21~0.72%, total Fe_2O_3 in the range of 1.33~6.06%, Al_2O_3 levels in the range of 12.98~17.14%, and Na_2O/K_2O ratios of 0.71~2.14. In a plot of total alkalis versus SiO_2 (TAS diagram; Figure 7a), sample points were present as the sub-alkaline series and plotted in diorite, granodiorite, and granite fields. This was a calc-alkaline series in a plot of K_2O versus SiO_2 (Figure 7b). Most samples on the SiO_2–(Na_2O+K_2O–CaO) diagram showed features of alkali–calcic and calc–alkali series (Figure 7d). Their A/CNK values ranged from 0.91 to 1.24, with an average of 1.05, indicating metaluminous and peraluminous characteristics on an A/NK versus A/CNK diagram (Figure 7c). Major element characteristics indicated an affinity with typical adakites, especially their high Na_2O contents (≥3.5%) with low K_2O/Na_2O ratios and a high-Al_2O_3 composition.
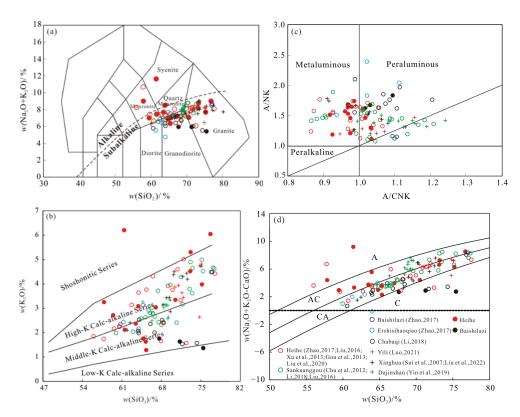
Figure 7. (**a**) Plot of the total alkali versus SiO_2 (TAS diagram) for granitoids in the Greater Khingan Mountains [41]; the boundary line between the alkaline and subalkaline series is from [42]; (**b**) SiO_2–K_2O diagram for granitoids in the Greater Khingan Mountains [43]; (**c**) A/CNK–A/NK diagram for granitoids in the Greater Khingan Mountains [44]; (**d**) SiO_2–($Na_2O + K_2O - CaO$) diagram for granitoids in the Greater Khingan Mountains [45]. (data of hollow circles and crosses are from [6,8,10,24,27–34]).A, alkaline series; AC, alkali–calcic series; CA, calc–alkaline series; C, calcic series.

The granitoids from Heihe, Baishilaiz, Sankuanggou, Ershisihaoqiao, and Chabaqi areas had SiO_2 in the range of 55.66~79.02% (n = 77), TiO_2 in the range of 0.04~1.02%, total Fe_2O_3 in the range of 0.32~10.29%, and Al_2O_3 in the range of 11.16~21.36%. In a plot of total alkalis versus SiO_2 (TAS diagram; Figure 7a), sample points were plotted in the diorite, granodiorite, and granite fields, with a small amount of (quartz) monzonite and syenite. These were a middle-K to high-K calc–alkaline series in a plot of K_2O versus SiO_2 (Figure 7b). Most samples on the SiO_2–(Na_2O+K_2O-CaO) diagram showed features of alkali–calcic and calc–alkali series (Figure 7d). The A/CNK values ranged from 0.86 to 1.21 with an average of 1.02, indicating metaluminous and peraluminous characteristics on an A/NK versus A/CNK diagram (Figure 7c).

4.2.3. Trace Elements

Trace element data of the granitoids are shown in Table S3. The granitoids from Xinghua, Yili, and Dajinshan areas were generally enriched in LILEs (e.g., Ba, U, K, and Sr) and depleted in HFSEs (e.g., Nb, Ta, P, and Ti) in a primitive mantle normalized spider diagram (Figure 8a); the depletion in Nb, Ta, and Ti indicates that hornblende and/or Fe–Ti oxides (e.g., rutile and ilmenite) are residual minerals. Zr–Hf is highly insoluble in hydrous fluids, resulting in negative anomalies of Zr–Hf in typical arc volcanic rocks. The granitoids generally characterized by positive Zr–Hf were likely from slab-derived melts rather than fluids [46]. These are characterized by an enrichment in light rare earth elements (LREEs) and a depletion in heavy rare earth elements (HREEs), ΣREE = 63.59~190.08 ppm, LREE/HREE = 10.66~40.90, $(La/Yb)_N$ = 11.70~71.11. The low HREE content can be interpreted as reflecting the presence of garnet ± hornblende in the partial melting residue

of their source [47]. When plotted as chondrite-normalized rare earth element patterns (Figure 8b), most samples displayed positive Eu anomalies. The frequently positive Sr and Eu anomaly indicates the lack of important plagioclase fractionation. Their $(La/Yb)_N > 10$, $Yb \leq 1.8$ ppm, $Y \leq 18$ ppm. Combined with the characteristics above-mentioned of the major elements, the presence of typical adakites is further indicated [47]. Moreover, they belong to high-SiO_2 adakites (HSA) because their Sr contents were lower than 1100 ppm and the MgO contents were generally less than 4% [48].
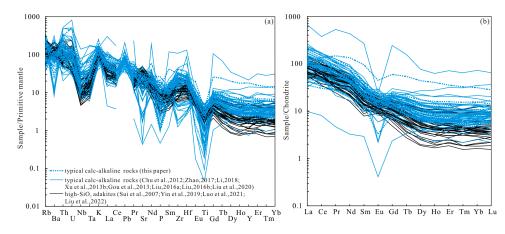

Figure 8. Primitive mantle normalized trace elements spider diagram (**a**) and chondrite-normalized REE pattern diagram (**b**) for Early Jurassic granitoids in the Greater Khingan Mountains. Data of solid lines are from [6,8,10,24,27–34].Chondrite and primitive mantle values were from [49] and [50], respectively.

The granitoids from the Heihe, Baishilazi, Ershisihaoqiao, Sankuanggou, and Chabaqi areas were generally enriched in LILEs (e.g., U, K, and Pb) and depleted in high-field-strength elements (HFSEs, e.g., Nb, Ta, P, and Ti), with the characteristics of arc magmatic rocks (Figure 8a). However, their ΣHREEs (4.93~134.06 ppm) were clearly higher than those of HSAs (ΣHREE = 2.96~15.05 ppm), with generally negative Sr and Eu anomalies (Figure 8), indicating typical calc-alkaline suprasubduction zone rocks.

4.2.4. Zircon Hf isotopes

Some of the zircon U–Pb dating spots for samples (quartz monzonite HEIH2018726–6 and porphyritic granite HEIH2018726–8) were chosen for in situ Hf isotope analysis (Table S4).

The initial $^{176}Hf/^{177}Hf$ ratios for primary zircons with the age of ~194 Ma in the porphyritic granite (HEIH2018726–8) sample varied from 0.282890 to 0.282971. The εHf(t) values and two-stage model ages (TDM_2) ranged from +7.8 to +10.7 and 528 to 707 Ma, respectively. The initial $^{176}Hf/^{177}Hf$ ratios for primary zircons with the age of ~183 Ma in quartz monzonite (HEIH2018726–6) sample varied from 0.282912 to 0.282942. Their εHf(t) values and two-stage model ages (TDM_2) ranged from +5.8 to +8.6 and from 650 Ma to 834 Ma, respectively.

5. Discussion

5.1. Age of Granitoid Formation

Xu et al. [4] divided the Mesozoic magmatism from NE China into six stages: Late Triassic (228~201 Ma), Early Jurassic (190~173 Ma), middle Late Jurassic (166~155 Ma), early Early Cretaceous (145~138 Ma), late Early Cretaceous (133~106 Ma), and Late Cretaceous (97~88 Ma); Wu et al. [3] suggested that the Mesozoic granitoids in NE China were mainly formed at ~115 Ma, 120~135 Ma, and 150~190 Ma; RIRGSH [11] proposed that large-scale granitoids distributed in the northeastern Xing'an massif were formed at T_3J_1. The LA–ICP–MS zircon U–Pb dating performed in this study indicated that Early Jurassic magmatism (~183 Ma, ~194 Ma) existed in the northern Greater Khingan Mountains. In addition, Gou et al. [28] indicated that a tonalite in the western Heihe area was formed at

181 ± 2 Ma. According to Zhao [10], a monzogranite in the Woniuhu area, a granodiorite in the Sanjianfang area, and a tonalite in the Baishilazi area were formed at 177 ± 1.0 Ma, 177.3 ± 1.2 Ma, and 171 ± 1.3 Ma, respectively. A monzogranite from the Woniuhu area was formed at 177.25 ± 0.45 Ma [32]. In this paper, the frequency distribution histogram (Figure 9) also indicates that a large number of granitoids formed during the Early Jurassic in the Greater Khingan Mountains. Moreover, the formation ages of some T_3J_1 batholiths marked by RIRGSH [11] were very rough and lacked accuracy. Based on our research and previous dating results, these batholiths should be further divided.
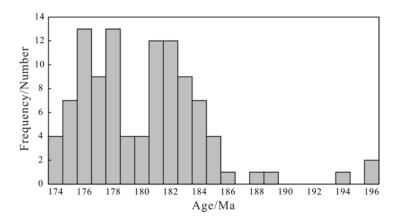

Figure 9. Zircon U–Pb age distribution histogram for the Early Jurassic granitoids in the Greater Khingan Mountains.

Current research indicates that Late Triassic magmatism only occurred sporadically in Huairou (236 ± 1Ma, monzogranite, [3]), Xintian (208 ± 2 Ma, felsic dyke, [51]), Guyuan (226 ± 2 Ma, plagioclase granite, [51]), and Duobaoshan (226.3 ± 2.3 Ma, tonalite, [52]) areas in the northern Greater Khingan Mountains, while large-scale granitoids were exposed around the Greater Khingan Mountains during the Early to Middle Jurassic [3,10,11,32]. Some batholiths in the northern Greater Khingan Mountains such as Baishushan and Heihuashan were formed in the Late Jurassic, [10,53]. In the Early Cretaceous, granitoids were mainly distributed along the boundary of the Xing'an massif in the NEE direction [3], with very frequent volcanism [4].

In addition, the exposed area of granitoids was sporadic before 188 Ma, with gradual increases in areal distribution at approximately 185 Ma, reaching the peak from 181 to 182 Ma. Moreover, during 176 to 178 Ma, another increase in the volume and areal distribution of granitoids occurred (Figure 9). This paper proposes that large-scale magmatism started no later than the Late Triassic, while in the Early Jurassic, the areal distribution of the granitoids increased greatly and formed peaks of 181 to 182 and 176 to 178 Ma, developing high numbers of granites. The magmatism lasted until the Early Cretaceous.

5.2. Rock Assemblages and Magma Sources

Condie and Benn [54] pointed out even in the Tertiary period, TTGs were an important juvenile component added to the continental crust in the Andes and other continental margin arcs. Barker [55] proposed that tonalite and trondhjemite suites also occurred on the continental margin during the Proterozoic, Paleozoic, Mesozoic, and Cenozoic Eras. Perhaps this is a more suitable way to view the ancient styles of subduction (Archean TTG) that have operated since at least 3.3 Ga, which persist in a limited way today [48]. Using CIPW norm mineral calculations can effectively distinguish tonalite and trondhjemite compared with QAP modal minerals [56]. Samples with quartz norm mineral >10% were plotted in An–Ab–Or classification diagrams (Figure 10); sample points fall into tonalite (T_1), trondhjemite (T_2), granodiorite (G_1), and granite rocks, indicating $T_1T_2G_1$ rock assemblages. The HSAs and calc-alkaline suprasubduction zone rocks proposed above do not conflict with the TTG rock assemblages here. The HSAs and calc-alkaline suprasubduction zone

rocks were judged by their geochemical characteristics and were a rock series, whereas the TTG assemblages were calculated by CIPW norm minerals as particular rocks. Thus, the HSAs and typical calc-alkaline suprasubduction zone rocks also belong to TTG rock assemblages (Figure 10).
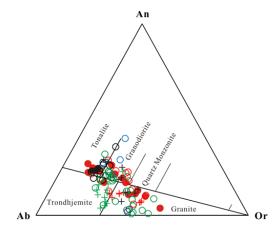

Figure 10. CIPW norm mineral classification diagram for Early Jurassic granitoids in the Greater Khingan Mountains [57] (legends are the same as in Figure 7).

Deng et al. [58] summarized the high P–T experiments on basaltic rocks on the basis of whether there was Pl in residual minerals, proposing that TTG melts formed under the pressure of 1500~1600 MPa can generally be regarded as the separation between higher-P and lower-P TTG rock assemblages. They also noted that the pressure and depth conditions of the MA series and LMA series (Figure 11) could be judged using the REE patterns, the Eu anomalies, and the Sr/Y versus Y diagram (Figure 12); then, the TTG subtypes can be divided. The granitoids in the Xinghua, Dajinshan, and Yili areas belong to the higher-pressure (P > 1500~1600 MPa) TTG subtype of MA, which are MA series on a plot of SiO_2 versus MgO (Figure 11) and shown as high Sr/Y and $(La/Yb)_N$, low Y and Yb_N features in the Sr/Y versus Y and $(La/Yb)_N$ versus Yb_N diagram (Figure 12), with generally weakly positive Eu anomalies or no Eu anomalies, indicating eclogite facies with an absence of plagioclase in residual minerals. The granitoids in Sankuanggou, Heihe, and Ershisihaoqiao to the southeast mostly have the characteristics of an LMA series (Figure 11) with low Sr/Y and La/Yb and high Y and Yb contents (Figure 12) with negative Eu anomalies (plagioclase as residual mineral), suggesting a lower-pressure (P < 1500~1600 MPa) TTG subtype of LMA.

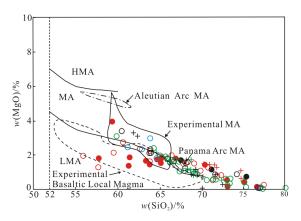**Figure 11.** Plot of SiO_2 versus MgO for the Early Jurassic granitoids in the Greater Khingan Mountains [58] (vertical dashed line indicates the boundary between basalt and andesite; the legends are the same as in Figure 7).
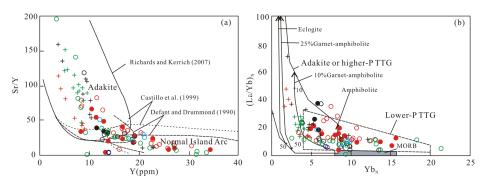
Figure 12. Plot of Sr/Y versus Y (**a**) and (La/Yb)$_N$ versus Yb$_N$ (**b**) for the Early Jurassic granitoids in the Greater Khingan Mountains (modified following [47,59–62]; the legends are the same as in Figure 7).

Magma sources can correspond to the hot crust and cold mantle model (Figure 13). Before subduction, the basaltic oceanic crust would be enriched in H$_2$O because of its interaction with sea water. When entering the deep part with slab subduction, it first metamorphosed to greenschist facies. Then, the ocean crust reached the boundary with amphibolite facies, released a lot of water to the mantle wedge and the upper crust, inducing metasomatic amphibole, but without partial melting, to generate magma. When further subducted to the boundary with eclogite, as a hot crust, it induced the dehydration and melting of amphibole from the oceanic crust, forming calc-alkaline arc magma (EM), with the pressure high enough to stabilize garnet (i.e., eclogite or garnet amphibolite), forming HSA series magma at the M point [48]. Then, magma ascended through the mantle wedge, reacting with peridotites to increase its content of MgO [58,63]. Finally, magma emplaced into the shallow crust (B point) or erupted out of the Earth's surface (V point). At the same time, magma reached the bottom of the crust, also inducing partial melting of the crust, forming calc-alkaline arc magma at the H point [64,65]. The HSA series from the Yili, Xinghua, and Dajinshan areas was shown as partial melting trends of 10% to 25% garnet–amphibolite (10:90 to 25:75), while parts of the calc-alkaline suprasubduction zone rocks represented partial melting trends in amphibolite (Figure 12b), further indicating the applicability of the cold mantle–hot crust model.

In addition, the ε(Hf) values and T$_{DM2}$ ages of zircons from two granitoids ranged from +5.6 to +10.7 and 528 to 834 Ma, respectively; the ε(Hf) values varied by 5.1 units (Figure 14); the T$_{DM2}$ ages were much older than the formation ages, suggesting that the sources could not be derived from a single component, and were explained by the MASH (melting, assimilation, storage, homogenization) model. Thus, the first batch of magma (i.e., ascendant magma from the partial melting of subducted oceanic crust) can immediately induce partial melting of the crust and magma formation, but the melting process will soon stop if there is not enough subsequent magma replenishment. The second batch of ascendant magma can cause the consolidated part (newly formed crust) to melt again and mix with the crust derived magma caused by the first batch ascendant magma, which is equivalent to the crust-derived magma being contaminated by the ascendant magma. In this way, the magma formed each time will be stored in a magma pool; then, homogenization of the magma chamber is realized due to diffusion and mixing, forming new magma with comparatively homogenous compositions [67,68].
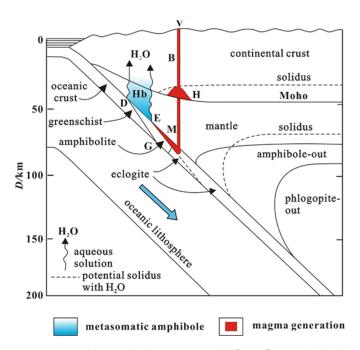
Figure 13. Cold mantle–hot crust model [58,66]. DG, dehydration front; DE, solutions enter the mantle along the DE; M, magma from subducted crust; H, additional magma from crustal rock; B, batholiths; V, volcanoes.
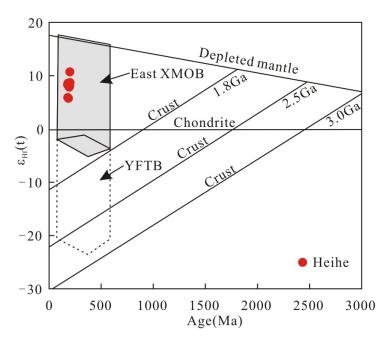

Figure 14. Correlations between the Hf isotopic compositions and ages of zircons from the Early Jurassic granitoids in the Greater Khingan Mountains [69]. XMOB, XingMeng Orogenic Belt; YFTB, Yanshan Fold and Thrust Belt.

5.3. Tectonic Setting of Early Jurassic Magmatism in the Greater Khingan Mountains

Tectonic settings of the Greater Khingan Mountains during the Early Jurassic are still in dispute. Sui et al. [8] considered that the Early Jurassic granitoids were similar to an active continental margin rock assemblage, which might be related to the Paleo-Pacific slab subduction. Based on their study of the Sankuanggou Fe–Cu deposit, Chu et al. [6] proposed that the deposit was formed in an island arc setting under the Paleo-Pacific subducted system and was closely associated with the early stage of the Paleo-Pacific Ocean subduction. Lin et al. [70] identified that the Mesozoic granites in the Greater Khingan

Mountains were constrained by a continental extension after the closure of the Paleo-Asian Ocean and a crust–mantle interaction during its closure stage. Gou et al. [28] indicated that the Early Jurassic granites in the Heihe and Sunwu areas were under a compressive setting associated with subduction of the Paleo-Pacific plate. Shao et al. [12] believed that the evolution of the Greater Khingan Mountains was related to the intracontinental orogenic mechanism and asthenosphere upwelling during the Mesozoic period. In addition, which ocean could be responsible for the large-scale exposed granitoids if the study area was subjected to ocean subduction in the Early Jurassic: the Paleo-Pacific Ocean or the Mongolia–Okhotsk Ocean [3,4,14,16–19]?

This paper suggests the granitoids were formed in a suprasubduction zone setting. The reasons are as follows. First, tonalite–trondhjemite–granodiorite (TTG) rock assemblages are the most important and typical igneous rock assemblages characterizing magmatic arcs related to ocean subduction [58,64]. The identification of TTG rock tectonic assemblages, enrichment in LILEs, and the depletion in HFSEs indicate the presence of ocean subduction. Second, sample points were plotted in the CA series (including the LF–CA series) on the TFeO/MgO versus SiO_2 diagram (Figure 15); the evolution of the TH series toward the CA series needs to be under the condition of water bearing, which is unique to the ocean subduction zone above the mantle [71]. Third, in the tectonic classification diagrams (Figure 16), the sample points were basically plotted in volcanic arc granites (VAGs), which also indicates a suprasubduction zone setting. Depending on the above evidence, we considered the Greater Khingan Mountains to be subjected to ocean subduction during the Early Jurassic period.
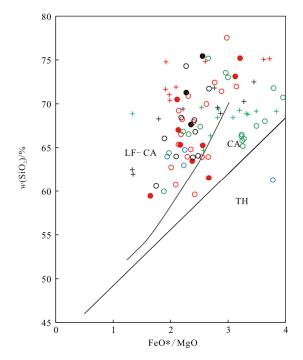

Figure 15. Plot of FeO*/MgO versus SiO_2 for the Early Jurassic granitoids in the Greater Khingan Mountains [71]. LF–CA, lower iron calc-alkaline series; CA, calc-alkaline series; TH, tholeiitic series. (the legends are the same as in Figure 7).
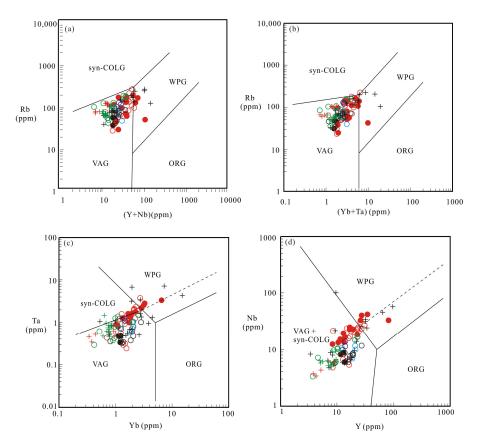
Figure 16. Tectonic classification diagrams of the Early Jurassic granitoids in the Greater Khingan Mountains [72]. (**a**) (Y + Nb), Rb diagram; (**b**) (Yb + Ta), Rb diagram; (**c**) Yb–Ta diagram; (**d**) Y–Nb diagram. Syn–COLG, syn–collisional granites; VAG, volcanic arc granites; ORG, oceanic ridge granites; WPG, within-plate granites (the legends are the same as in Figure 7).

When was the eastern part of the Mongolia–Okhotsk Ocean finally closed? Paleomagnetic studies conducted by Pei et al. [73] and Enkin et al. [74] indicated that the Mongolia–Okhotsk Ocean was still open by ~3000 km in its eastern part at ca. 155 Ma; closure of the Ocean occurred in the Late Jurassic, although Kravchinsky [75] proposed that the closure of the Mongol–Okhotsk Ocean began in the Permian period, and complete closure in its eastern part occurred from the Late Jurassic to Early Cretaceous. Others support the final closure of its eastern part in the Late Jurassic to Early Cretaceous [76] and the Early Cretaceous [9], based on evidence from the Late Mesozoic volcanic rocks. Accordingly, we hypothesize that the eastern part of the Mongolia–Okhotsk Ocean was still in its continuous subducted stage in the Early Jurassic period.

In terms of rock assemblages, those around the Heihe, Baishilazi, Dajinshan, and Xinghua areas were mainly TTG formations, whereas those in the Yili, Sankuanggou, and Chabaqi areas were mainly GG and G assemblages. In an active continental margin environment, TTG assemblages were formed adjacent to the ocean, whereas GG and G assemblages were formed adjacent to the continent [71]. The northeastern Heihe, Baishilazi, and Xinghua areas as well as the westward Dajinshan area were adjacent to the ocean and formed an outer subduction zone, whereas the southwestward Sankuanggou, Yili, and Chabaqi areas were adjacent to the continent, forming an inner subduction zone. The orientation of the magmatic front can indicate a subduction direction; the direction opposite to the magmatic front is a direction of ocean subduction [65]. Thus, we can roughly infer a southward and southwestward subduction event that was related to the Mongolia–Okhotsk Ocean. Tang et al. [77] identified that the distribution directions of the Early Jurassic igneous rocks on the Erguna and Xing'an massifs were nearly parallel to the Mongolia–Okhotsk

suture zone, which also indicated that the ocean should be the Mongolia–Okhotsk Ocean to the north rather than the Paleo-Pacific Ocean to the east.

6. Conclusions

(1) Zircon U–Pb dating of granitoids from the northern Greater Khingan Mountains indicated that they were formed in 183.1 ± 1.3 Ma and 194.2 ± 1.4 Ma, namely, the Early Jurassic period. According to the temporal and spatial distributions of the rocks, we can conclude that Mesozoic magmatism occurred sporadically in the Late Triassic period, then reached the peak period with a more areal distribution of granitoids in the Early to Middle Jurassic; relatively active magmatism lasted until the Early Cretaceous.

(2) The Early Jurassic granitoids were identified as TTG rock assemblages using the CIPW norm minerals calculation method. These were generally medium-potassium calc-alkali series and high-potassium calc-alkali series, metaluminous and peraluminous rocks. Most of them belonged to alkali–calcic and calc-alkali series rocks. Granitoids were enriched in LILEs, depleted in HFSEs, and characterized by arc intrusive rocks. Rock assemblages and geochemical characteristics indicated a direct relationship with ocean subduction.

(3) The above-mentioned TTGs can be further divided into higher-pressure TTG subtypes of the MA series (corresponding to the HSA series) and lower-pressure TTG subtypes of the LMA series (corresponding to the calc-alkaline suprasubduction zone rock series). The former were presumably produced by the partial melting of young and hot oceanic crust under eclogite to garnet amphibolite facies conditions, whereas the latter were produced by the partial melting of subducted oceanic crust under garnet-free amphibolite facies conditions with shallower depths and lower pressure and the partial melting of the sub-arc crust.

(4) It is speculated that granitoids were formed under the influence of southward and southwestward subduction of the Mongolia–Okhotsk Ocean in the north of the Xing'an massif according to their spatial distributions.

References

1. Huang, S.Q.; Dong, S.W.; Zhang, F.Q.; Miao, L.C.; Zhu, M.S. Tectonic Deformation and Dynamic Characteristics of the Middle Part of the Mongolia-Okhotsk Collisional Belt, Mongolia. *Acta Geosci. Sin.* **2014**, *35*, 415–424. [CrossRef]

2. Xu, W.L.; Sun, C.Y.; Tang, J.; Luan, J.P.; Wang, F. Basement Nature and Tectonic Evolution of the Xing'an-Mongolian Orogenic Belt. *Earth Sci.* **2019**, *44*, 1620–1646. [CrossRef]

3. Wu, F.Y.; Sun, D.Y.; Ge, W.C.; Zhang, Y.B.; Grant, M.L.; Wilde, S.A. Geochronology of the Phanerozoic Granitoids in Northeastern China. *J. Asian Earth Sci.* **2011**, *41*, 1–30. [CrossRef]

4. Xu, W.L.; Pei, F.P.; Wang, F.; Meng, E.; Ji, W.Q.; Yang, D.B.; Wang, W. Spatial-temporal relationships of Mesozoic volcanic rocks in NE China: Constraints on tectonic overprinting and transformations between multiple tectonic regimes. *J. Asian Earth Sci.* **2013**, *74*, 167–193. [CrossRef]

5. Jiang, S.H.; Zhang, L.L.; Liu, Y.F.; Liu, C.H.; Kang, H.; Wang, F.X. Metallogeny of Xing-Meng Orogenic Belt and some related problems. *Miner. Depos.* **2018**, *37*, 671–711. [CrossRef]

6. Chu, S.X.; Liu, J.M.; Xu, J.H.; Wei, H.; Chai, H.; Tong, K.Y. Zircon U-Pb Dating, Petrogenesis and Tectonic Significance of the Granodiorite in the Sankuanggou Skarn Fe-Cu Deposit, Heilongjiang Province. *Acta Petrol. Sin.* **2012**, *28*, 433–450.

7. Wang, F.; Zhou, X.H.; Zhang, L.C.; Ying, J.F.; Zhang, Y.T.; Wu, F.Y.; Zhu, R.X. Late Mesozoic volcanism in the Great Xing'an Range (NE China): Timing and implications for the dynamic setting of NE Asia. *Earth Planet. Sci. Lett.* **2006**, *251*, 179–198. [CrossRef]

8. Sui, Z.M.; Ge, W.C.; Wu, F.Y.; Zhang, J.H.; Xu, X.C.; Cheng, R.Y. Zircon U-Pb ages, geochemistry and its petrogenesis of Jurassic granites in northeastern part of the Da Hinggan Mts. *Acta Petrol. Sin.* **2007**, *23*, 461–480.

9. Shao, S.; Deng, J.F.; Liu, C.; Zhao, Y.D.; Duan, P.X.; Xu, F.M.; Di, Y.J. Geochemical characteristics and tectonic setting of Early Cretaceous volcanic rocks in the Heihe area, Heilongjiang Province, China. *Earth Sci. Front.* **2018**, *25*, 215–229.

10. Zhao, Y.D. Disintegration of Metamorphic Basement and Petrogenesis of Late Paleozoic and Jurassic Granitoids in the Northeastern Xing'an Massif. Doctoral Dissertation, China University of Geoscience Beijing, Beijing, China, 2017.

11. RIRGSH (Research Institute of Regional Geological Survey of Heilongjiang). *Regional Geological Survey Report of the People's Republic of China—Map of Heihe*; Research Institute of Regional Geological Survey of Heilongjiang: Harbin, China, 2009; pp. 1–369.

12. Shao, J.A.; Zhang, L.Q.; Xiao, Q.H.; Li, X.B. Rising of Da Hinggan Mts in Mesozoic: A Possible Mechanism of Intracontinental Orogeny. *Acta Petrol. Sin.* **2005**, *21*, 789–794.

13. Xu, W.L.; Ji, W.Q.; Pei, F.P.; Meng, E.; Yu, Y.; Yang, D.B.; Zhang, X.Z. Triassic volcanism in eastern Heilongjiang and Jilin provinces, NE China: Chronology, geochemistry, and tectonic implications. *J. Asian Earth Sci.* **2009**, *34*, 392–402. [CrossRef]

14. Deng, C.Z.; Sun, D.Y.; Han, J.S.; Chen, H.Y.; Li, G.H.; Xiao, B.; Li, R.C. Late-stage southwards subduction of the Mongol-Okhotsk oceanic slab and implications for porphyry Cu-Mo mineralization: Constraints from igneous rocks associated with the Fukeshan deposit, NE China. *Lithos* **2019**, *326–327*, 341–357. [CrossRef]

15. Tang, J.; Xu, W.L.; Wang, F.; Wang, W.; Xu, M.J.; Zhang, Y.H. Geochronology and geochemistry of Neoproterozoic magmatism in the Erguna Massif, NE China: Petrogenesis and implications for the breakup of the Rodinia supercontinent. *Precambrian Res.* **2013**, *224*, 597–611. [CrossRef]

16. Sun, D.Y.; Gou, J.; Wang, T.H.; Ren, Y.S.; Liu, Y.J.; Guo, H.Y.; Liu, X.M.; Hu, Z.C. Geochronological and geochemical constraints on the Erguna massif basement, NE China-subduction history of the Mongol-Okhotsk oceanic crust. *Int. Geol. Rev.* **2013**, *55*, 1801–1816. [CrossRef]

17. Sun, G.S.; Zhao, T.X.; Jin, R.X.; Wang, Q.H. Zircon U-Pb chronology, geochemistry, and petrogenesis of the high Nb–Ta alkaline rhyolites at the Tuohe Tree Farm, northern Volcanic Belt, Great Xing'an Range, China. *Can. J. Earth Sci.* **2019**, *56*, 1001–1016. [CrossRef]

18. Fu, J.Y.; Na, F.C.; Li, Y.C.; Sun, W.; Zhong, H.; Yang, H.; Yang, X.P.; Zhang, G.Y.; Liu, Y.C.; Yang, Y.J. Southward subduction of the Mongo-Okhotsk Ocean: Middle Triassic magmatic records of the Luomahu Group in northwest of Lesser Khingan Mountains. *Geol. Bull. China* **2021**, *40*, 889–904. [CrossRef]

19. Li, Z.Q.; Chen, J.L.; Zou, H.; Wang, C.S.; Meng, Q.A.; Liu, H.L.; Wang, S.Z. Mesozoic-Cenozoic tectonic evolution and dynamics of the Songliao Basin, NE Asia: Implications for the closure of the Paleo-Asian Ocean and Mongol-Okhotsk Ocean and subduction of the Paleo-Pacific Ocean. *Earth-Sci. Rev.* **2021**, *218*, 1–26. [CrossRef]

20. Han, G.Q.; Liu, Y.J.; Neubauer, F.; Bartel, E.; Genser, J.; Feng, Z.Q.; Zhang, L.; Yang, M.C. U–Pb age and Hf isotopic data of detrital zircons from the Devonian and Carboniferous sandstones in Yimin area, NE China: New evidences to the collision timing between the Xing'an and Erguna blocks in eastern segment of Central Asian Orogenic Belt. *J. Asian Earth Sci.* **2015**, *97*, 211–228. [CrossRef]

21. Ge, W.C.; Wu, F.Y.; Zhou, C.Y.; Abdel-Rahman, A.A. Emplacement age of the Tahe granite and its constraints on the tectonic nature of the Ergun block in the northern part of the Da Hinggan Range. *Chin. Sci. Bull.* **2005**, *50*, 2097–2105. [CrossRef]

22. Cui, F.H.; Zheng, C.Q.; Xu, X.C.; Yao, W.G.; Shi, L.; Li, J.; Xu, J.L. Late Carboniferous Magmatic Activities in the Quanshenglinchang Area, Great Xing'an Range: Constrains on the Timing of Amalgamation between Xing'an and Songnen Massifs. *Acta Geol. Sin.* **2013**, *87*, 1247–1263.

23. Li, T.D.; Liu, Y.; Ding, X.Z.; Pang, J.F. Ten advances in regional geological research of China in recent years. *Acta Geol. Sin.* **2022**, *96*, 1544–1581. [CrossRef]

24. Li, Y. Geochronology and Geochemistry of the Mesozoic Igneous Rocks in the Xing'an Massif, NE China: Constraints on the Evolution of the Mongol–Okhotsk Tectonic Regime. Doctoral Dissertation, Jilin University, Changchun, China, 2018.

25. Pan, G.T.; Lu, S.N.; Xiao, Q.H.; Zhang, K.X.; Yin, F.G.; Hao, G.J.; Luo, M.S.; Ren, F.; Yuan, S.H. Division of tectonic stages and tectonic evolution in China. *Earth Sci. Front.* **2016**, *23*, 1–23. [CrossRef]

26. She, H.Q.; LI, J.W.; Xiang, A.P.; Guan, J.D.; Yang, Y.C.; Zhang, D.Q.; Tan, G.; Zhang, B. U-Pb ages of the zircons from primary rocks in middle-northern Daxinganling and its implications to geotectonic evolution. *Acta Petrol. Sin.* **2012**, *28*, 571–594.

27. Xu, M.J.; Xu, W.L.; Wang, F.; Gao, F.H.; Yu, J.J. Geochronology and geochemistry of the Early Jurassic granitoids in the central Lesser Xing'an Range, NE China and its tectonic implications. *Acta Petrol. Sin.* **2013**, *29*, 354–368.

28. Gou, J.; Sun, D.Y.; Li, R.; Wei, H.Y.; Wang, T.H.; Liu, X.M.; Hu, Z.C. Geochronology, Geochemistry and Petrogenesis of the Early Mesozoic Granites in the Sunwu–Jiayin Area, Heilongjiang Province. *J. Jilin Univ. (Earth Sci. Ed.)* **2013**, *43*, 119–133. [CrossRef]

29. Liu, Y.J. Geochemistry and Implications for Tectonic Evolution of Mesozoic Granite in Woduhe area, Northern Daxing'an Mountains. Master's Thesis, Jilin University, Changchun, China, 2016.

30. Liu, J.Y. The Geochronological and Geochemical Research of Granites in Sandaowanzi, Heilongjiang Province. Master's Thesis, China University of Geoscience Beijing, Beijing, China, 2016.

31. Yin, Z.G.; Li, M.; Li, W.L.; Zhang, H.; Zhang, S.T.; Gong, Z.M.; Li, H.N.; Hao, K.; Pang, X.C. The Origin and Tectonic Environment of the Early Jurassic Adakitic Granodiorite in the Dajinshan Area of the Central and Northern Da Hinggan Range. *Bull. Mineral. Petrol. Geochem.* **2019**, *38*, 69–79. [CrossRef]

32. Liu, J.X.; Liu, C.; Deng, J.F.; Luo, Z.H.; Zhang, Y.; He, G.Q.; Liu, Q.; Yue, H.J. Igneous Rock Records and Genesis of the Early Jurassic Magmatic Arc in Heihe Area of Heilongjiang Province. *Earth Sci.* **2020**, *45*, 2538–2554. [CrossRef]

33. Luo, N.G.; Gao, L.F.; Zhang, J.; Zhang, Z.G.; Yin, Z.G.; Xie, Z.; Cui, J.Y.; Wu, Z.J. U-Pb age and geochemical characteristics of the Early Jurassic monzogranite in Yili area, Northern Great Hinggan Mountains, and their tectonic implications. *Geol. Rev.* **2021**, *67*, 1649–1669. [CrossRef]

34. Liu, B.; Wang, Y.D.; Wen, Y.Q.; Han, B.F. Geochronology and Geochemistry of Mesozoic Igneous Rocks in the Hanjiayuanzi–Fulin Area of the Erguna Massif: Constrains on the Tectonic Evolution of the Mongol-Okhotsk Ocean. *Earth Sci.* **2022**, *47*, 3316–3333. [CrossRef]

35. Zhang, L.L.; Zhu, D.C.; Wang, Q.; Zhao, Z.D.; Liu, D.; Xie, J.C. Late Cretaceous Volcanic Rocks in the Sangri Area, Southern Lhasa Terrane, Tibet: Evidence for Oceanic Ridge Subduction. *Lithos* **2019**, *326–327*, 144–157. [CrossRef]

36. Anderson, T. Correction of common Lead in U–Pb analyses that do not report ^{204}Pb. *Chem. Geol.* **2002**, *192*, 59–79. [CrossRef]

37. Liu, Y.S.; Hu, Z.C.; Gao, S.; Günther, D.; Xu, J.; Gao, C.G.; Chen, H.H. In Situ Analysis of Major and Trace Elements of Anhydrous Minerals by LA–ICP–MS without Applying an Internal Standard. *Chem. Geol.* **2008**, *257*, 34–43. [CrossRef]

38. Ludwig, K.R. ISOPLOT 3: A geochronological toolkit for microsoft excel. *Berkeley Geochronol. Cent. Spec. Publ.* **2003**, *4*, 74.

39. Wu, F.Y.; Yang, Y.H.; Xie, L.W.; Yang, J.H.; Xu, P. Hf isotopic compositions of the standard zircons and baddeleyites used in U–Pb geochronology. *Chem. Geol.* **2006**, *234*, 105–126. [CrossRef]

40. Wu, Y.B.; Zheng, Y.F. Zircon Genetic Mineralogy and Its Constraints on U–Pb Age Interpretation. *Chin. Sci. Bull.* **2004**, *49*, 1589–1604. [CrossRef]

41. Middlemost, E.A.K. Naming Materials in the Magma/Igneous Rock System. *Earth-Sci. Rev.* **1994**, *37*, 215–224. [CrossRef]

42. Irvine, T.N.; Baragar, W.R.A. A Guide to the Chemical Classification of the Common Volcanic Rocks. *Can. J. Earth Sci.* **1971**, *8*, 523–548. [CrossRef]

43. Peccerillo, R.; Taylor, S.R. Geochemistry of Eocene Calc-Alkaline Volcanic Rocks from the Kastamonu Area, Northern Turkey. *Contrib. Mineral. Petrol.* **1976**, *58*, 63–81. [CrossRef]

44. Maniar, P.D.; Piccoli, P.M. Tectonic Discrimination of Granitoids. *Geol. Soc. Am. Bull.* **1989**, *101*, 635–643. [CrossRef]

45. Frost, B.R.; Barnes, C.G.; Collins, W.J.; Arculus, R.J.; Ellis, D.J.; Frost, C.D. A Geochemical Classification for Granitoids Rocks. *J. Petrol.* **2001**, *42*, 2033–2048. [CrossRef]

46. Zhang, G.L.; Zhang, J.; Dalton, H.; Phillips, D. Geochemical and Chronological Constraints on the Origin and Mantle Source of Early Cretaceous Arc Volcanism on the Gagua Ridge in Western Pacific. *Geochem. Geophys. Geosyst.* **2022**, *23*, e2022GC010424. [CrossRef]

47. Martin, H. Adakitic magmas: Modern analogues of Archaean granitoids. *Lithos* **1999**, *46*, 411–429. [CrossRef]

48. Martin, H.; Smithies, R.H.; Rapp, R.; Moyen, J.-F.; Champion, D. An overview of adakite, tonalite–trondhjemite–granodiorite (TTG), and sanukitoid: Relationships and some implications for crustal evolution. *Lithos* **2005**, *79*, 1–24. [CrossRef]

49. Boynton, W.V. Geochemistry of the rare earth elements: Meteorite studies. In *Rare Earth Element Geochemistry*; Henderson, P., Ed.; Elsevier: Amsterdam, The Netherlands, 1984; pp. 63–114.

50. Sun, S.S.; McDonough, W.F. Chemical and isotopic systematics of ocneanic basalts: Implications for mantle composition and processes. In *Magmatism in Ocean Basins*; Saunders, A.D., Norry, M.J., Eds.; Geological Society of Special Publication: London, UK, 1989; pp. 313–345.

51. Miao, L.C. *SHRIMP Zircon Geochronological Studies of the Da Hinggan Mountains*; Report of the Postdoctoral Research, Institute of Geology and Geophysics; Chinese Academy of Sciences: Beijing, China, 2003.

52. Liu, B.S.; Cheng, Z.X.; Qian, C.; Zhang, C.P.; Zhong, H.; Han, R.P. Geochronology and Geodynamic Background Study of the Late Triassic Bimodal Pattern Intrusive Rock in Da Hinggan Mountains Duobaoshan Area. *Earth Sci.* **2021**, *46*, 2311–2328. [CrossRef]

53. He, G.Q.; Liu, C.; Deng, J.F.; Luo, Z.H.; Zhang, Y.; Liu, J.X.; Liu, Q.; Yue, H.J. Records of the Late Jurassic Magmatic Arc in Heihe Area, Heilongjiang Province: Discussion on the Relationship with Mongolia–Okhotsk Ocean. *Earth Sci.* **2020**, *45*, 2524–2537. [CrossRef]

54. Condie, K.C.; Benn, K. Archean Geodynamics: Similar to or Different from Modern Geodynamics? *Geophys. Monogr. Ser.* **2006**, *164*, 47–59. [CrossRef]

55. Barker, F. *Trondhjemites, Dacites and Related Rocks*; Elsevier: New York, NY, USA, 1979.

56. Feng, Y.F.; Deng, J.F.; Xiao, Q.H.; Xing, G.F.; Su, S.G.; Cui, X.Y.; Gong, F.Y. Recognizing the TTG Rock Types: Discussion and Suggestion. *Geol. J. China Univ.* **2011**, *17*, 406–414. [CrossRef]

57. O'Connor, J.T. A Classification for Quartz-Rich Igneous Rocks Based on Feldspar Ratios. *USGS Prof. Pap.* **1965**, *525*, 79–84.

58. Deng, J.F.; Liu, C.; Di, Y.J.; Feng, Y.F.; Xiao, Q.H.; Liu, Y.; Ding, X.Z.; Meng, X.G.; Huang, F.; Zhao, G.C.; et al. Discussion on the Tonalite-Trondhjemite-Granodiorite (TTG) Petrotectonic Assemblage and Its Subtype. *Earth Sci. Front.* **2018**, *25*, 42–50. [CrossRef]

59. Defant, M.J.; Drummond, M.S. Derivation of some modern arc magmas by melting of young subducted lithosphere. *Nature* **1990**, *347*, 662–665. [CrossRef]

60. Richards, J.P.; Kerrich, R. Special paper: Adakite-like rocks: Their diverse origins and questionable role in metallogenesis. *Econ. Geol.* **2007**, *102*, 537–576. [CrossRef]

61. Castillo, P.; Janney, P.; Solidum, R. Petrology and geochemistry of Camiguin Island, southern Philippines: Insights to the source of adakites and other lavas in a complex arc setting. *Contrib. Mineral. Petrol.* **1999**, *134*, 33–51. [CrossRef]

62. Martin, H. Effect of steeper Archaean geothermal gradient on geochemistry of subduction-zone magmas. *Geology* **1986**, *14*, 753–756. [CrossRef]

63. Deng, J.F.; Liu, C.; Feng, Y.F.; Xiao, Q.H.; Su, S.G.; Zhao, G.C.; Kong, W.Q.; Cao, W.Y. High magnesian andesitic/dioritic rocks (HMA) and magnesian andesitic/dioritic rocks (MA): Two igneous rock types related to oceanic subduction. *Geol. China* **2010**, *37*, 1112–1118. [CrossRef]

64. Deng, J.F.; Luo, Z.H.; Su, S.G.; Mo, X.X.; Yu, B.S.; Lai, X.Y.; Zhen, H.W. *Petrogenesis, Tectonic Setting and Mineralization*; Geological Publishing House: Beijing, China, 2004; pp. 1–381.

65. Deng, J.F.; Feng, Y.F.; Di, Y.J.; Liu, C.; Xiao, Q.H.; Su, S.G.; Zhao, G.C.; Meng, F.; Ma, S.; Yao, T. Magmatic Arc and Ocean–Continent Transition: Discussion. *Geol. Rev.* **2015**, *61*, 473–484. [CrossRef]

66. Wyllie, P.J. Constraints Imposed by Experimental Petrology on Possible and Impossible Magma Sources and Products. *Philos. Trans. R. Soc. Lond. Ser. A Math. Phys. Sci.* **1984**, *310*, 439–456. [CrossRef]

67. Hildreth, W. Quaternary magmatism in the Cascades: Geological perspectives. *USGS Prof. Pap.* **2007**, *1744*, 1–125. [CrossRef]

68. Luo, Z.H.; Lu, X.X.; Chen, B.H.; Li, M.L.; Liao, T.; Huang, F.; Yang, Z.F. *Introduction to Transmagmatic Fluid Mineralization*; Geological Publishing House: Beijing, China, 2009; pp. 1–180.

69. Yang, J.H.; Wu, F.Y.; Shao, J.A.; Wilde, S.A.; Xie, L.W.; Liu, X.M. Constraints on the timing of uplift of the Yanshan Fold and Thrust Belt, North China. *Earth Planet. Sci. Lett.* **2006**, *246*, 245–336. [CrossRef]

70. Lin, Q.; Ge, W.C.; Wu, F.Y.; Sun, D.Y.; Cao, L. Geochemistry of Mesozoic granites in Da Hinggan Ling ranges. *Acta Petrol. Sin.* **2004**, *20*, 403–412.

71. Deng, J.F.; Xiao, Q.H.; Su, S.G.; Liu, C.; Zhao, G.C.; Wu, Z.X.; Liu, Y. Igneous Petrotectonic Assemblages and Tectonic Settings: A Discussion. *Geol. J. China Univ.* **2007**, *13*, 392–402. [CrossRef]

72. Pearce, J.A.; Harris, N.B.W.; Tindle, A.G. Trace Element Discrimination Diagrams for the Tectonic Interpretation of Granitoids. *J. Petrol.* **1984**, *25*, 956–983. [CrossRef]

73. Pei, J.L.; Sun, Z.M.; Liu, J.; Liu, J.; Wang, X.S.; Yang, Z.Y.; Zhao, Y.; Li, H.B. A paleomagnetic study from the Late Jurassic volcanics (155 Ma), North China: Implications for the width of Mongol–Okhotsk Ocean. *Tectonophysics* **2011**, *510*, 370–380. [CrossRef]

74. Enkin, R.J.; Yang, Z.Y.; Chen, Y.; Courtillot, V. Paleomagnetic constraints on the geodynamic history of China from the Permian to the present. *J. Geophys. Res.* **1992**, *97*, 13953–13989. [CrossRef]

75. Kravchinsky, V.A.; Konstantinov, K.M.; Cogne, J.-P. Palaeomagnetic study of Vendian and Early Cambrian rocks of South Siberia and Central Mongolia: Was the Siberian platform assembled at this time? *Precambrian Res.* **2001**, *110*, 61–92. [CrossRef]

76. Zhou, X.H.; Ying, J.F.; Wang, F.; Zhang, L.C.; Wilde, S.A.; Badamgarav, J.; Badarch, G. Late Mesozoic Volcanism Across E, Mongolia and Da Hinggan Mts, NE China: Timing constraint on the closure of Mongol-Okhotsk Sea. *Geochim. Cosmochim. Acta* **2006**, *70*, A753. [CrossRef]

77. Tang, J.; Xu, W.L.; Wang, F.; Ge, W.C. Subduction history of the Paleo–Pacific slab beneath Eurasian continent: Mesozoic–Paleogene magmatic records in Northeast Asia. *Sci. China Earth Sci.* **2018**, *48*, 549–583. [CrossRef]